Quantification of angiogenic sprouting under different growth factors in a microfluidic platform

Cristina Del Amo [a,1], Carlos Borau [a,1], Raquel Gutiérrez [a], Jesús Asín [b], José Manuel García-Aznar [a,n]

[a] *Multiscale in Mechanical and Biological Engineering (M2BE), Aragón Institute of Engineering Research (I3A), Department of Mechanical Engineering, University of Zaragoza, Zaragoza, Spain*

[b] *Department of Statistical Methods, University of Zaragoza, Zaragoza, Spain*

Angiogenesis, as example of collective migration of endothelial cells (ECs), is the main dynamic process that culminates in sprout formation from existing vessels. After tissue injury, the vascularity is inter- rupted, triggering the regeneration process and the release of different growth factors (GFs). The main aim of this work is to quantify the effect of specific GFs during the initial stage of sprout formation, namely: VEGF, PDGF-BB, TGFβ and BMP-2, all of them involved in regenerative processes. For this purpose, we designed a novel algorithm implemented in Matlab to quantify the advance of the EC mono- layer over time and the sprout structure in 3D. Our results show that VEGF is the main regulatory GF on angiogenesis processes, producing longer sprouts with higher frequency. However, the chemoattractant effect of VEGF depends on its concentration and its spatiotemporal location, having a critical impact on the sprout time evolution. PDGF-BB (namely as PDGF) has a global negative effect on both the number and length of sprouts. TGFβ enhances sprout length at earlier times, although its effect gradually disappears over time. Finally, BMP-2 produces, overall, less number and shorter sprouts, but was the only GF with a positive evolution at longer times, producing fewer but longer sprouts.

Keywords: Sprouting Angiogenesis Growth factors Microfluidics Collective Cell Migration

1. Introduction

Regeneration processes occur in all living tissues after some injury or damage is produced. The regeneration of the global vascular network and its connection with the damaged tissue is one of the first steps to restore the tissue functionality (Huttala et al., 2015; Johnson and Wilgus, 2014).

Angiogenesis is the process of new blood vessel growth from preexisting ones (Chung et al., 2014; Daub and Merks, 2013; Jung and Kleinheinz, 2013; Park et al., 2014) and it is mainly guided by VEGF (Vascular Endothelial Growth Factor) gradients, one of the most potent proangiogenic GFs (Bentley et al., 2009; Johnson and Wilgus, 2014; Shamloo et al., 2008), and other signals such as oxygen (Decaris et al., 2009; Vempati et al., 2014). Chemotactic and polarizing effects of VEGF have been thoroughly analyzed in previous works (Shamloo et al., 2008) and its relevance inducing sprout formation have been confirmed by many research works (Blanco and Gerhardt, 2013; Farahat et al., 2012; Feng et al., 2013; Johnson and Wilgus, 2014; Vempati et al., 2014).owever, there are other GFs implicated in tissue vasculariza- tion such as TGFβ (Human Transforming Growth Factor-Beta), PDGF-BB (Human Platelet Derived Growth Factor-BB, henceforth referred as PDGF) and BMP (Bone Morphogenetic Protein) among others. For instance, PDGF is implicated in osteogenesis, acting as mitogen for osteoblast and increasing VEGF expression (Jung and Kleinheinz, 2013). The secretion of PDGF in fracture healing con- tributes to marrow stromal cells recruitment, which may in turn increase the liberation of other angiogenic factors (Cenni et al., 2011; Park et al., of molecular signalization involved in angiogenesis (Theberge et al., 2015). However, to the best of our knowledge, none of them have analyzed under similar conditions the temporal effect of several GFs on angiogenesis. In this work, we aim to quantify the capacity of four different GFs involved in angiogenic processes (namely VEGF, PDGF, TGF, and BMP-2), to promote sprouting in a collagen type I scaffold which replicates the ECM microenvironment. To evaluate the angiogenic effect on the ECs monolayer, we measured the frequency and the length of the formed sprouts during 24 h.

2013). Additionally, PDGF stabilizes blood vessels by recruiting of pericytes, whereas VEGF promotes EC growth (Banfi et al., 2012). Regarding TGFβ, its proangiogenic effect depends on assay conditions. In vivo, TGFβ contributes to the stimulation of macrophages which release angiogenic factors, whereas in vitro, TGFβ inhibits the ECs growth and proliferation, thus decreasing the sprout formation (Tonnesen et al., 2000). The main factor involved in bone regeneration is BMP-2 (Human Bone Morphogenetic Protein), which affects EC proliferation and migration (Pardali and Ten Dijke, 2012) and promotes the chemotaxis and differentiation towards the osteogenic pathway (Ribeiro et al., 2015). In Table 1, we show a summary of the main impact of the GFs on tissue regeneration.

In recent years, microfluidic devices have gained great popularity due to the easy reproduction, control and monitoring of a wide variety of microenvironmental factors. In fact, these devices have been used to reproduce fundamental aspects of angiogenesis, such as those presented by Jeon et al. (2013) and Zervantonakis et al. (2012) to simulate wound healing or tumor growth. Other works using similar microdevices have been focused on regeneration processes such as the generation of 3D capillary beds in vitro (Chan et al., 2012), anti-angiogenesis drug screening (Kim et al., 2015) or on cellular dynamics to analyze cell migration in sprouting processes (Vickerman et al., 2008).

In addition, the high versatility of PDMS to design different cell culture platforms and protocols has allowed the analysis

2. Materials and methods

2.1. Microfluidic device

The geometry and fabrication of microdevices was based on the methods implemented by Farahat et al. (2012). These devices present a central chamber filled with hydrogel, and two lateral channels for cell seeding (EC channel) and the supply of different growth factors (GF channel) (see Fig. 1 for geometric details).

2.2. Collagen hydrogel scaffold in a microfluidic assay

The collagen hydrogel was prepared from type I collagen gel solution (Corning Collagen I, Rat Tail. 3 mg/ml) at 2.5 mg/ml following the methodology proposed by Farahat et al. (2012) and Zervantonakis et al. (2012), with phosphate buffered saline (PBS; Lonza), NAOH and EGM2 (Endothelial Cell Growth Media, Lonza). It was softly pipetted into the devices and polymerized for 40 min in a humid chamber, at 37 °C and 5% CO_2. After that, the matrix was hydrated and incubated overnight at the same conditions. The mechanical properties of 2.5 mg/ml collagen gels have been characterized in literature (Antoine et al., 2014; Miron-Mendoza et al., 2010; Zuidema et al., 2014), presenting a storage modulus $G^0 \sim 18$ Pa. In regards to the transport properties of these gels, and according to the measurements of Farahat et al. (2012) , GF concentration decreases almost linearly from the source channel and across the collagen, with a diffusion coefficient of $5e^{-11}$ m^2/s. Using the same protocol, Zervantonakis et al. (2012) found the diffusive permeability to range from 0.7570.093e^{-7} m/s to 4.087 1.11e^{-7} m/s. Further quantification of GF gradients in collagen can be found in Farahat et al. (2012) and Moreno-Arotzena et al. (2014).

2.3. Cell culture and seeding

Human Umbilical Vein Endothelial Cells (HUVEC, C2519A, Lonza) in passages 3–8 and 70–90% confluence were seeded in the microfluidic devices with a concentration of 1.5 x 10^6 cell/ml. Endothelial cell growth media (EGM-2, Lonza) was used as cell culture medium.

Table 1
Summary of the impact of different GFs on cell and tissue behavior.

Growth factor (GF)	Characteristics	Effects	References
Vascular Endothelial Growth Factor (VEGF)	Some isoforms: VEGF-A, VEGF-B, VEGF-C, VEGF-D and PlGF(placental growth factor) *VEGF-A: homodimer with a molecular weight of* 40 kDa *and* 165 *amino acid residues/subunit.*	Cell Proliferation, migration, differentiation Increasing of vascular permeability, formation of new blood vessels	Blanco and Gerhardt (2013), Johnson and Wilgus (2014), and Tonnesen et al. (2000).
Human Platelet Derived Growth Factor-BB (*PDGF-BB*)	Protein of 24.3 kDa, a disulfide-linked homodimer of two chains of 218 amino acids	Cell proliferation, angiogenesis and fibrosis recruitment and proliferation of pericytes during angiogenesis	Rong et al. (2015), and Ucuzian et al. (2010).
Human Transforming Growth Factor- Beta 1 (*TGFβ1*)	Protein of 25 kDa synthesized by human platelets, has a central role in cell growth regulation, differentiation and function.	Cell proliferation, migration and capillary tube formation	Pardali and Ten Dijke (2012), and Ucuzian et al. (2010).
Human Bone Morphogenetic Protein (*BMP2*)	Protein with 26 kDa belonging to the TGFβ superfamily	Bone formation growth, differentiation, chemotaxis and apoptosis.	Ribeiro et al. (2015), Suwanadabol et al. (2012), and Willette et al. (1999).

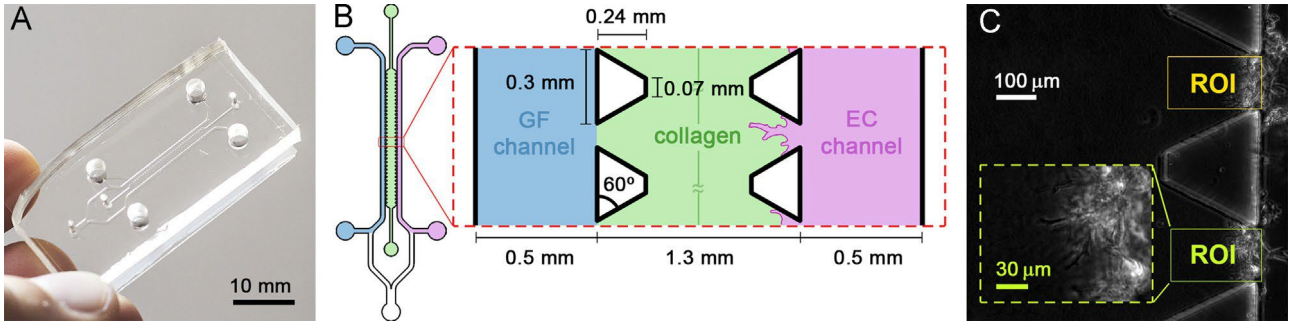

Fig. 1. (A) Self-made microfluidic device prototype used in our assays. Geometry was obtained from the work of Farahat et al. (2012). (B) Top view and inset of the device geometry with a central chamber (green) and two lateral channels (blue: growth factor (GF channel), pink: endothelial cell seeding (EC channel)). Channel and pillar heights (and therefore gel thickness) are 120 micrometer. (C) Example image from the experiments: cells forming sprouts between two micropillars of the device. Yellow and green windows are the actual regions of interest (ROIs) submitted to analysis. (For interpretation of the references to color in this figure legend, the reader is referred to the web version of this article.)

Firstly, we used EGM2 to equilibrate the microdevices, which had been treated in the previous 24 h, and incubated them for 2 h. Secondly, 20 ml of ECs suspension were filled by a previously dried lateral channel (Fig. S1A). The seeded devices were placed in a humid box for 40 min and oriented vertically to promote the deposition of cells on the collagen hydrogel (Fig. S1B). After cell incubation, the EC channel was washed to remove the surplus cells, hence leaving a monolayer (Fig. S1C). Finally, the growth factors were added at the GF channel. Conditions used in each assay are shown in Table 2.

Table 2
Different GFs conditions found in the literature that have been applied in microfluidics-based experiments of angiogenesis. Concentration of GFs at each channel. *EGM-2: Endothelial cell growth media.

Condition	GF channel	EC channel	References
0-0	EGM-2*	EGM-2	–
0-vegf	EGM-2	40 ng/ml [VEGF]	Kim et al. (2015)
vegf-0	40 ng/ml	EGM-2	–
vegf-vegf	50 ng/ml [VEGF]	40 ng/ml [VEGF]	Qutub and Popel (2009)
tgfb-vegf	10 ng/ml [TGFβ]	40 ng/ml [VEGF]	Schreier et al. (1993)
pdgf-vegf	10 ng/ml [PDGF]	40 ng/ml [VEGF]	Schreier et al. (1993)
bmp-vegf	2 ng/ml [BMP-2]	40 ng/ml [VEGF]	Kramer et al. (2000)

2.4. Design of experiment

The experiment was designed to obtain enough samples for each condition so that the statistical analysis was able to distinguish specific effects of the different GFs. Application of VEGF only in the EC channel was chosen as the reference/control condition (*0-vegf*). Each additional condition (*vegf-vegf*, *tgfb-vegf*, *pdgf-vegf*, *bmp-vegf*) was replicated 4 times, always accompanied by a control experiment (*0-vegf*). Finally, to isolate the effects of VEGF and complete the study, 2 replicates of the null condition (*0-0*) and 2 of the control-inverted condition (*vegf-0*) were performed (See Table 3).

2.5. Sprout tracking and quantification

Two hours after ECs seeding and GFs incorporation, cell tracking was initiated in the monolayer and maintained for 24 h with 37 °C, 95% humidity and 5% of CO_2 conditions. Phase contrast images were captured every 20 min.

Table 3
Main descriptive indicators: number of replicates per condition, number of processed ROIs, total number of measured sprouts, percentage of sprouts longer than 30 mm, mean length, standard deviation and skewness of the distribution. Note the different number of ROIs per condition due to the variability in the number of finally selected regions caused by the disposal of invalid samples.

Condition	# Replicates	# ROIs	# Sprouts	% Length430	Length (mm)		
					Mean	Sd	Skewness
0-0	2	22	22,947	2.7	9.01	8.66	3.65
0-vegf	16	66	90,814	13.9	16.48	18.72	2.67
vegf-0	2	16	23,260	28.7	25.79	25.76	2.02
vegf-vegf	4	25	26,255	13.4	16.77	18.56	3.28
tgfb-vegf	4	28	28,907	6.7	11.74	13.23	3.02
pdgf-vegf	4	24	22,229	12.7	15.47	18.62	2.78
bmp-vegf	4	14	18,788	8.9	12.76	14.81	2.96

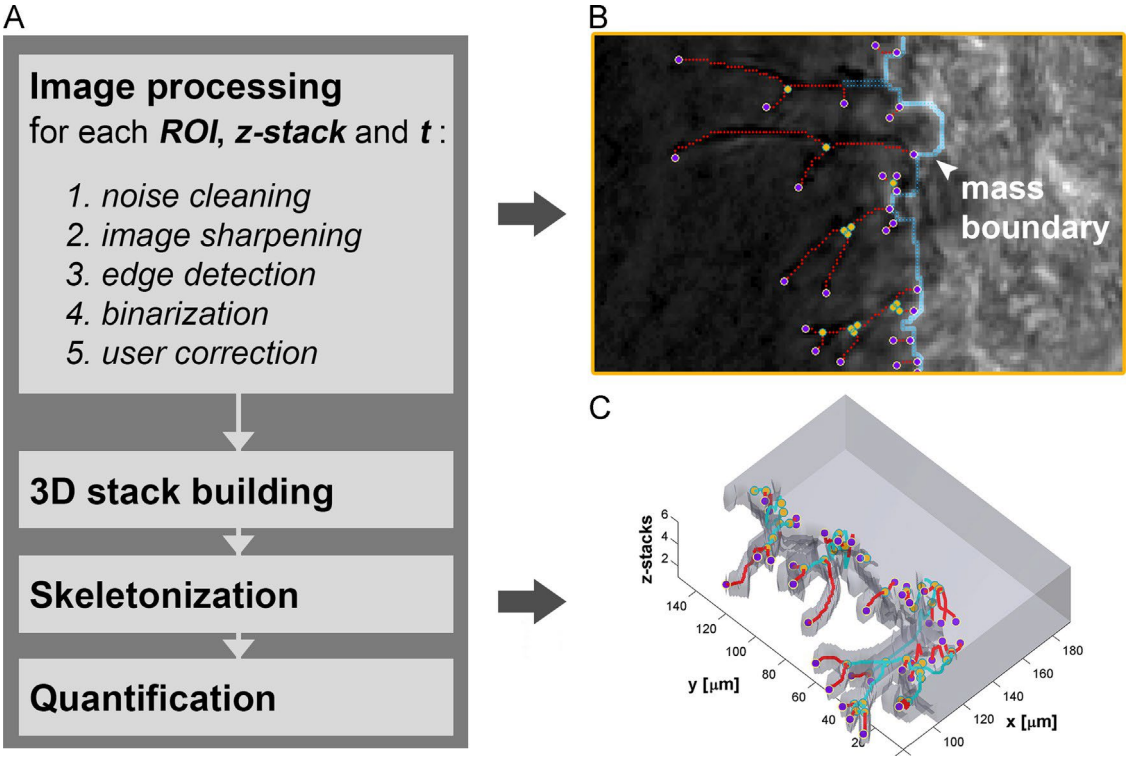

Fig. 2. (A) Workflow scheme of the developed image-processing code. (B) Image shown to the user for manual correction. When necessary, the user is allowed to draw masks to add/remove specific regions so that the script can re-process the image. Purple/yellow circles represent end/branch points of the computed 2D sprouts. Red dots represent pixels corresponding to sprouts. Light blue line highlights the cell mass boundary (leading edge), used as reference to measure the sprout lengths. (C) 3D reconstruction of the z-stacks at a specific time step. Semi-transparent gray represents the cell mass, whereas cell sprouts are plotted as red/cyan segments. These segments are colored in red when they join a branch-point with an end-point, and in cyan when they join two branch-points. This coloring method provides visual information regarding the sprout network complexity, although both type of segments are considered equivalent for the numerical quantification. (For interpretation of the references to color in this figure legend, the reader is referred to the web version of this article.)

Each microdevice has 36 micropillars alongside the EC channel, and therefore there are 37 regions of interest (ROIs) to quantify cell sprouting (Fig. 1C). Among all of them, up to 16 ROIs per replicate were selected, although only those regions of higher image quality were kept for processing. Each of these ROIs represents 10 z-stacks (one slice every 20 mm) overtime (about 70 frames). In sum, we processed up to 195 ROIs, or in other words more than $1.35e^5$ images, and measured more than $2.3e^5$ sprouts (See Table 3). For this analysis, we developed a hand-coded script with a graphical interface using Matlab. This script automatically cleans the noise from the input images and segments background from cell mass by using different filters (Fig. 2A). Besides, it permits the user to define masks to correct or discard any frame or part of it if necessary (eg. highly blurred captures). Fig. 2B shows an example of an image seen by the user while checking the frames. Once this process is finished, the z-stacks of each temporal frame are joined in a 3D volume which skeleton is computed (Lee et al., 1994) (see Fig. 2C). Finally, all the necessary data is automatically collected for the statistical analysis. More details regarding the implementation of the image processing can be found in Supplementary material.

2.6. Statistical analysis

Statistical hypothesis tests were performed in order to analyze the significance of differences between sprouting length distributions under different conditions. An elevated sample size of sprouts was obtained for all conditions, ranging from 18,788 to 90,814 (See Table 3). The skewed right distribution shown in Fig. 3 implies that non-parametric tests based on ranks were the best option to compare distributions. Firstly, Kruskall–Wallis (KW) tests were used to check the null hypothesis establishing that the length distribution is unchanged regarding the conditions. Secondly, when the null was rejected at 0.01 significance level, a multiple comparison test (simultaneous confidence level of 95%) was applied to distinguish conditions that were significantly different (see in Fig. S2, S3, S4).

3. Results

3.1. Measurements of VEGF-induced sprouting

To test the effect of VEGF on the EC monolayer, four different conditions were used: (i) null concentration in both channels (*0-0*), (ii) VEGF only in the ECs channel (*0-vegf*), (iii) VEGF only in the GFs channel (*vegf-0*) and (iv) VEGF in both channels (*vegf-vegf*).

To perform our analysis, we created the following two groups of results: (i) all sprouts and (ii) only long sprouts. A sprout was considered long when its 3D length was higher than 30 mm. We choose this threshold since HUVEC cell size usually range between 20–40 mm (Bauer et al., 2009). Additionally, we measured our cells confirming that their medium size was in the same range.

The distribution of length of all sprouts is remarkably skewed under all conditions (Fig. 3, Table 3), with condition (*vegf-0*) having the greatest dispersion. In spite of their similarities, a median test (Kruskal–Wallis) confirmed that all the groups had mean ranks significantly different among each other ($p < 0.01$) (Fig. S2).

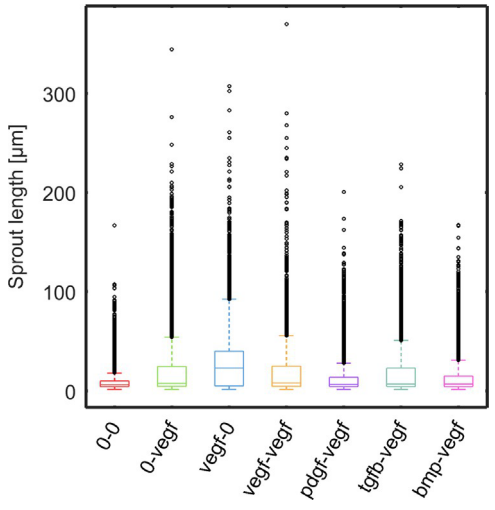

Fig. 3. Length distribution of all sprouts for each condition. All the cases show an asymmetric distribution with high values (up to 300 mm). Condition (*vegf-0*) presents the greatest dispersion whereas condition (*0-0*) has the most concentrated data.

The frequency of sprout formation was tracked over time every 20 min. Compared to condition (*0-vegf*), condition (*0-0*) produced a similar amount of sprouts (Fig. 4A), however, very few of them were long (Fig. 4B). Condition (*vegf-0*) presented the greatest number of sprouts during the first half of the experiment (Fig. 4A), although its effect was reduced over time. However, the number of long sprouts was higher during the whole period (Fig. 4B), which is reflected in the significantly higher number of total sprouts per ROI (Fig. 4C). The opposite effect was observed in condition (*vegf-vegf*) where the growth of sprouts was minimal at the beginning, but increased with time until the number of long sprouts was the highest among all conditions (Fig. 4B). On average, the total number of long sprouts was similar (no significant differences) compared to condition (*0-vegf*) (Fig. 4C).

Overall, sprout length distribution was highly concentrated at low values, so that the frequency of long sprout formation was rather low. In any case, the mean sprout length over time was higher for condition (*vegf-0*), lower for condition (*0-0*), and similar for condition (*vegf-vegf*) compared to the condition (*0-vegf*) (Fig. 4D).

3.2. Chemotactic effect of nonspecific angiogenic factors

We analyzed whether specific GFs of wound healing (PDGF and TGFβ) or bone regeneration (BMP2) could stimulate the vessel formation.

The negative effect of nonspecific angiogenic factors was neatly observed, especially in the frequency of sprout formation. The number of sprouts for conditions (*pdgf-vegf*), (*tgfb-vegf*) and (*bmp-vegf*) was significantly lower compared to condition (*0-vegf*) during most of the time (Fig. 4A, C), being this difference more critical for long sprouts. In fact, in these conditions, long sprouts practically disappeared at the end of the experiment (Fig. 4B).

Regarding sprout lengths, the trends were similar to those observed in the frequency data, with these conditions getting overall shorter sprouts compared to condition (*0-vegf*). However, condition (*bmp-vegf*) showed an interesting behavior during the last hours of the experiment. While the number of sprouts was greatly reduced compared to the initial times, the length of these sprouts was larger, even superior to those produced in the condition (*0-vegf*) (Fig. 4D).

3.3. Quantification of failed sprouts

For the successful formation of sprouts, cells make many attempts, some of them succeed but others do not. Since we aimed to quantify the number of failed attempts in each ROI, we counted the number of cells loosed from the cell mass (the monolayer) trying to create a new sprout. Some of the tip cells left the monolayer and some returned to it after a while. However, at the moment they were unattached, we assessed them as a failed sprout. As shown in Fig. 5, although the median value of loosed cells was different for all conditions compared to condition (*0-vegf*), only condition (*tgfb-vegf*) presented significant differences. Overall, conditions including VEGF as GF ((*0-vegf*), (*vegf-0*) *and* (*vegf-vegf*)) did not promote the migration of individual cells and therefore the connection between cells was maintained over time. In fact, looking together at the high number of loosed cells of conditions (*pdgf-vegf*), (*tgfb-vegf*) and (*bmp-vegf*) (Fig. 5), and their low number of long sprouts produced (Fig. 4), suggests a direct relationship between the propensity of cells to get unattached from the monolayer and the frequency of successful sprouts.

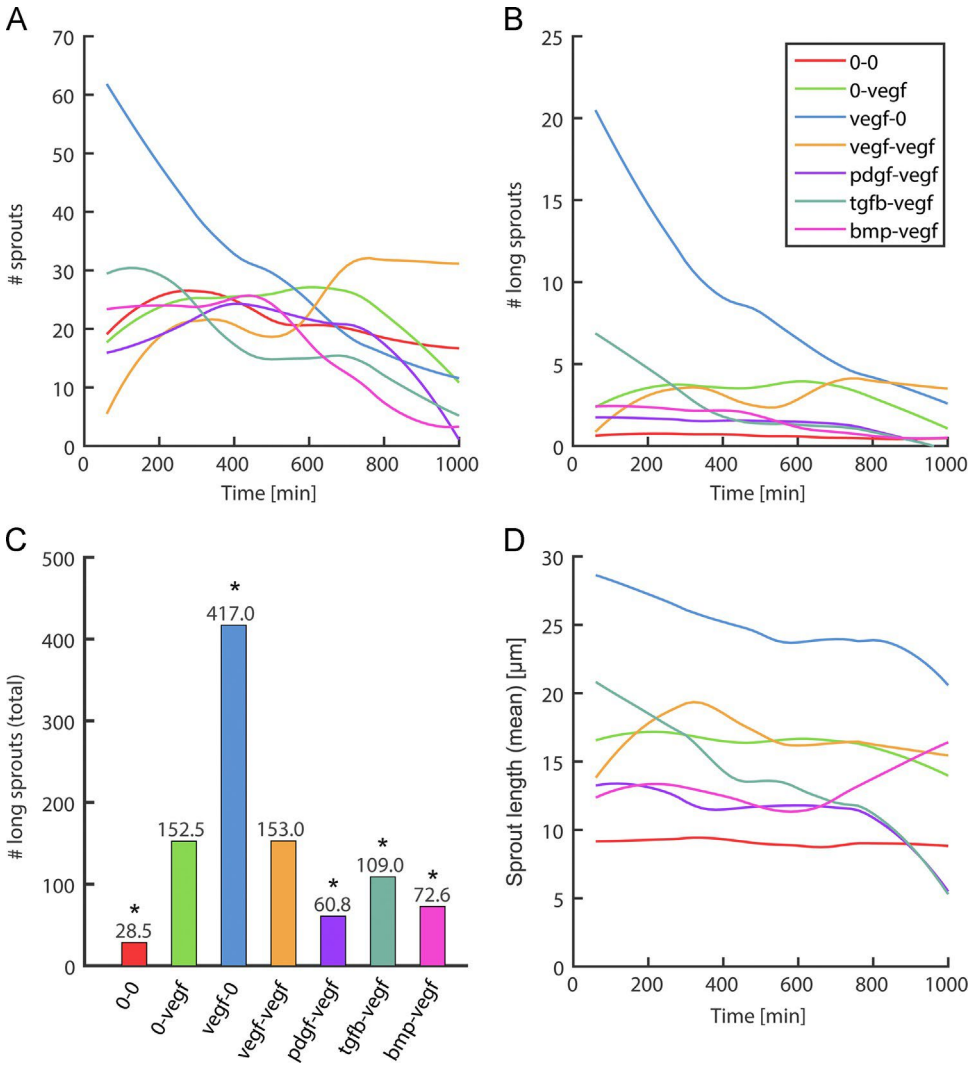

Fig. 4. Number of sprouts (A) and long sprouts 430 mm (B) per ROI over time. (C) Total number of long sprouts per ROI. * indicates (p 0.01) in a Kruskal–Wallis median test (Fig. S4). (D) Mean of the sprout length distribution over time. Panels A, B and D share legend and are plotted using a r-Loess smoothing filter. At earlier times, condition (*vegf-0*) produced the largest number of sprouts (A), a third of which were long (B). This effect gradually disappeared, yet the number of observed long sprouts was higher compared to the case (*0-vegf*) at the end of the experiments. Condition (*vegf-vegf*) reduced the number of sprouts (both short and long) at the beginning, although this effect was reversed as time advanced, producing the highest number of sprouts during the last steps. The other conditions, had negative effects on the number of sprouts produced, which almost disappeared in the last hours. Overall, condition (*vegf-0*) produced a significant higher number of long sprouts (C) which is reflected in a higher value of the mean sprout length over time (D). Condition (*vegf-vegf*) was similar to the condition (*0-vegf*) with no significant differences in the total number of sprouts. Mean values of sprout length were slightly higher at the end of the experiment. Conditions (*pdgf-vegf*), (*tgfb-vegf*) and (*bmp-vegf*) presented overall fewer and shorter sprouts compared to condition (*0-vegf*), critically decreasing the sprout length at later times except for condition (*bmp-vegf*) which, interestingly, produced longer sprouts during the last hours (D).

4. Discussion

This study aimed to analyze the paracrine effects of GFs commonly released by different cell types (epithelial cells, ECs or osteogenic cells) on the formation of novel angiogenic sprouts.

From our experiments, we clearly concluded that the application of VEGF in the GF channel significantly enhanced the angiogenic response compared to non-specific factors. The generation of a chemoattractant gradient in the direction of sprout growth, (*condition* (*vegf-0*)), promoted sprouting and cell reorganization, producing longer sprouts with higher frequency. This effect was stronger at earlier times (Fig. 4A,B,D). As time progressed and the concentration of VEGF decreased due to degradation, the number of sprouts as well as their length decreased, although the number of long sprouts and the mean sprout length kept at higher values compared to the condition (*0-vegf*) (Fig. 4B,D).

To test the effect of VEGF when present in both channels, we created a concentration gradient between the GF and the EC channel (*condition* (*vegf-vegf*)). The initial decrease in sprout formation (Fig. 4A,B) suggests a saturation of VEGF receptors in ECs, not responding to the chemoattractant signal probably due to the distortion of DII4/Notch signaling activity (Blanco and Gerhardt, 2013; Carlier et al., 2012). In any case, sprout formation frequency was recovered, and the number of long sprouts was the highest among all the conditions during the last hours (Fig. 4B). Mean sprout length was similar, and sometimes higher than the condition (*0-vegf*) (Fig. 4C). The average number of loose cells was similar compared to the condition (*0-vegf*) (Fig. 5), suggesting that the overexposure to VEGF may inhibit sprouting but still does not promote single cell migration.

The endothelium secretes several GFs such as PDGF and it may act in an autocrine or a paracrine way, amplifying the angiogenic response (Fox and Gasparini, 2001). In previous studies, PDGF was determined to affect EC indirectly by inducing the release of VEGF (Li et al., 2005). Moreover, Banfi et al. (2012) concluded that the co-expression of VEGF and PDGF was able to induce efficacious

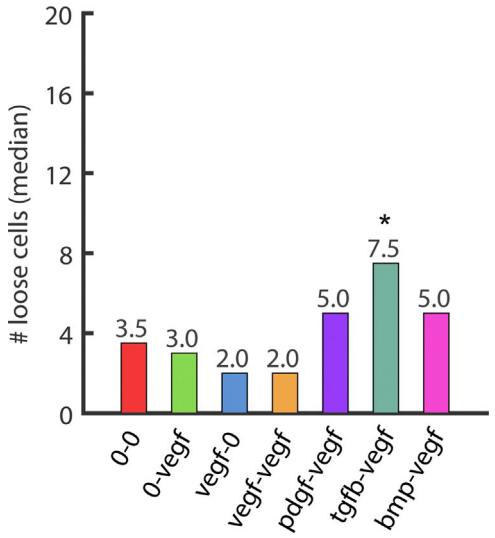

Fig. 5. Number of single cells detached from the main cell mass in each ROI. Compared to the condition (*0-vegf*), the number of cells that failed to form a sprout was lower for conditions (v*egf-0*) and (v*egf-vegf*), and higher for the rest of them, although the difference was statistically significant only for condition (*tgfb-vegf*) ($p \leq 0.01$) (Fig. S4).

angiogenesis. However, our results showed the negative effect of condition (*pdgf-vegf*) on sprout development. This could be explained by the non-optimal balance of concentration between PDGF and VEGF and the inappropriate spatiotemporal gradient. In fact, in some kinds of tumors, the recruitment and proliferation of pericytes (special vascular cells) increase the PDGF expression but do not increase the vascular development (Bhowmick et al., 2004).

TFGβ may promote tumor growth by enhancing angiogenesis (Bhowmick et al., 2004). Previous works have demonstrated that shallow gradients of TGFβ (0.5–2 ng/ml) show no discernable effect on sprout formation (Nakatsu et al., 2003). Our results revealed that the effect of higher concentrations of TGFβ (10 ng/ml) was neither relevant on angiogenic processes. In fact, there was a significant high number of loose cells (failed sprouts) suggesting that single cell migration is promoted, which could explain the low effectiveness of this GF to form long sprouts.

Previous reports have shown the modest effect of BMP2 on HUVEC migration and therefore on sprout formation (Willette et al., 1999). In our results we confirmed this inhibiting effect, although we observed a delayed effect leading to the formation of long sprouts at final phases. The number of loose cells was similar to (*pdgf-vegf*) assay, presenting the same behavior regarding sprout formation and elongation.

We developed our own software to quantify sprouting from microscopy images, which provided us freedom and total adaptability for the required analysis. It is worth noting that despite the potential of our code, it presents some limitations, since its effectiveness relies on image quality. Blurriness, brightness, water drops due to condensation or other image artifacts require specific attention and adjustments. Additionally, the image-processing workflow is time-consuming. While the automatic processes present almost no computational cost (a few hours at most to build the 3D volume and measure the sprouts of a whole microdevice), the time required by the user to check specific frames and add the proper masks may reach weeks of work.

To summarize, our results show that VEGF is the main proangiogenic factor, able to stimulate the sprout formation especially when applied in the GF channel, opposite to the EC monolayer. This fact indicates that the induction of a VEGF gradient enhances the angiogenesis process. The chemoattractant effect of this growth factor could be employed for instance to accelerate regenerative processes, which could be crucial for tissue regenerative purposes. On the other hand, TFGβ was found to be the main factor inhibiting sprout formation and thus, it could be used to suppress the angiogenic process in tumor expansion. The effect of the rest of non-specific factors (PDGF and BMP2) were not relevant to enhance sprouting, although the effect of BMP at longer times should be further studied to better understand its behavior.

Our workbench allows a fine control of the conditions applied, such as the GF concentration and gradient and the fluid flow. In fact, several studies have shown the mechanical influence of fluid flow, inducing shear stress to the endothelial cells and significantly affecting branching, capillarisation (Hernández Vera et al., 2009), sprout promotion (Galie et al., 2014; Vickerman and Kamm, 2012) or vessel formation (Song and Munn, 2011; Vickerman et al., 2008). Hence, due to the importance of interstitial fluid on angiogenic development, we will combine GFs with fluid flow in future experiments. Furthermore, instead of using exogenous GFs, we aim to co-culture different cell types to analyze their effect on angiogenesis.

Acknowledgments

The authors would like to thank Dr. Roger Kamm, Dr. William J. Polacheck and Dr. Ioannis K. Zervantonakis for their collaboration with techniques. This work was supported by the European Research Council (ERC) through Project ERC-2012-StG 306751, the Spanish Ministry of Economy and Competitiveness (DPI2012-38090-C03-01) and the Ministry of Education, Culture and Sports, Spain (FPU13/03194). We would like also to thank the Aragón Government through the European Social Fund.

References

Antoine, E.E., Vlachos, P.P., Rylander, M.N., 2014. Review of collagen I hydrogels for bioengineered tissue microenvironments: characterization of mechanics, structure and transport. Tissue Eng. Part B Rev. 20, 683–696.

Banfi, A., von Degenfeld, G., Gianni-Barrera, R., Reginato, S., Merchant, M.J., McDonald, D.M., Blau, H.M., 2012. Therapeutic angiogenesis due to balanced single-vector delivery of VEGF and PDGF-BB. FASEB J. : Off. Publ. Fed. Am. Soc. Exp. Biol. 26, 2486–2497.

Bauer, A.L., Jackson, T.L., Jiang, Y., 2009. Topography of extracellular matrix mediates vascular morphogenesis and migration speeds in angiogenesis. PLoS Comput. Biol. 5.

Bentley, K., Mariggi, G., Gerhardt, H., Bates, P. a, 2009. Tipping the balance: robustness of tip cell selection, migration and fusion in angiogenesis. PLoS Comput. Biol. 5, e1000549.

Bhowmick, N.A., Neilson, E.G., Moses, H.L., 2004. Stromal fibroblasts in cancer initiation and progression. Nature, 432.

Blanco, R., Gerhardt, H., 2013. VEGF and notch in tip and stalk cell selection. Cold Spring Harb. Perspect. Med. 3, 1–19.

Carlier, A., Geris, L., Bentley, K., Carmeliet, G., Carmeliet, P., Van Oosterwyck, H., 2012. MOSAIC: a multiscale model of osteogenesis and sprouting angiogenesis with lateral inhibition of endothelial cells. PLoS Comput. Biol. 8, e1002724.

Cenni, E., Perut, F., Baldini, N., 2011. In vitro models for the evaluation of angiogenic potential in bone engineering. Acta Pharmacol. Sin. 32, 21–30.

Chan, J.M., Zervantonakis, I.K., Rimchala, T., Polacheck, W.J., Whisler, J., Kamm, R.D., 2012. Engineering of in vitro 3D capillary beds by self-directed angiogenic sprouting. PLoS One 7, 1–11.

Chung, S., Sudo, R., Vickerman, V., Zervantonakis, I.K., Kamm, R.D., 2014. Microfluidic platforms for studies of angiogenesis. Cell Migr. Cell–Cell Interact. Access. Biomed. Eng. Soc.

Daub, J.T., Merks, R.M.H., 2013. A cell-based model of extracellular-matrix-guided endothelial cell migration during angiogenesis. Bull. Math. Biol. 75, 1377–1399.

Decaris, M.L., Lee, C.I., Yoder, M.C., Tarantal, A.F., Leach, J.K., 2009. Influence of the oxygen microenvironment on the proangiogenic potential of human endothelial colony forming cells. Angiogenesis 12, 303–311.

Farahat, W.A., Wood, L.B., Zervantonakis, I.K., Schor, A., Ong, S., Neal, D., Kamm, R.D., et al., 2012. Ensemble analysis of angiogenic growth in three-dimensional microfluidic cell cultures. PloS One 7, e37333.

Feng, X., Tonnesen, M.G., Mousa, S.A., Clark, R.A.F., 2013. Fibrin and collagen differentially but synergistically regulate sprout angiogenesis of human dermal microvascular endothelial cells in 3-dimensional matrix. Int. J. Cell Biol. 2013, 231279.

Fox, S., Gasparini, G.H.A., 2001. Angiogenesis: pathological, prognosis, and their link to trial design and anticancer drugs. Lancet Oncol. 2, 278–289.

Galie, P.A., Nguyen, D.-H.T., Choi, C.K., Cohen, D.M., Janmey, P.A., Chen, C.S., 2014. Fluid shear stress threshold regulates angiogenic sprouting. Proc. Natl. Acad. Sci. USA 111, 7968–7973.

Hernández Vera, R., Genové, E., Alvarez, L., Borrós, S., Kamm, R., Lauffenburger, D., Semino, C.E., 2009. Interstitial fluid flow intensity modulates endothelial sprouting in restricted Src-activated cell clusters during capillary morphogenesis. Tissue Eng. Part A 15, 175–185.

Huttala, O., Vuorenpää, H., Toimela, T., Uotila, J., Kuokkanen, H., Ylikomi, T., Sarkanen, J.-R., et al., 2015. Human vascular model with defined stimulation medium —a characterization study. Altex 32, 125–136.

Jeon, J.S., Zervantonakis, I.K., Chung, S., Kamm, R.D., Charest, J.L., 2013. In vitro model of tumor cell extravasation. PloS One 8, e56910.

Johnson, K.E., Wilgus, T. a, 2014. Vascular Endothelial Growth Factor and angiogenesis in the regulation of cutaneous wound repair. Adv. Wound Care 3, 647–661.

Jung, S., Kleinheinz, J., 2013. Angiogenesis : the fundament of osseous regeneration. Hard Tissue 2, 1–4.

Kim, C., Kasuya, J., Jeon, J., Chung, S., Kamm, R.D., 2015. A quantitative microfluidic angiogenesis screen for studying anti-angiogenic therapeutic drugs. Lab Chip 15, 301–310.

Kramer, J., Hegert, C., Guan, K., Wobus, A.M., Müller, P.K., Rohwedel, J., 2000. Embryonic stem cell-derived chondrogenic differentiation in vitro: activation by BMP-2 and BMP-4. Mech. Dev. 92, 193–205.

Lee, T.C., Kashyap, R.L., Chu, C.N., 1994. Building skeleton models via 3-D medial surface axis thinning algorithms. CVGIP. Graph. Models Image Process. 56, 462–478.

Li, X., Tjwa, M., Moons, L., Fons, P., Noel, A., Ny, A., Zhou, J.M., et al., 2005. Revascularization of ischemic tissues by PDGF-CC via effects on endothelial cells and their progenitors. J. Clin. Investig. 115, 118–127.

Miron-Mendoza, M., Seemann, J., Grinnell, F., 2010. The differential regulation of cell motile activity through matrix stiffness and porosity in three dimensional collagen matrices. Biomaterials 31, 6425–6435.

Moreno-Arotzena, O., Mendoza, G., Cóndor, M., Rüberg, T., García-Aznar, J.M., 2014. Inducing chemotactic and haptotactic cues in microfluidic devices for three-dimensional in vitro assays. Biomicrofluidics 8, 064122.

Nakatsu, M.N., Sainson, R.C.A., Aoto, J.N., Taylor, K.L., Aitkenhead, M., Pérez-del-Pulgar, S., Carpenter, P.M., et al., 2003. Angiogenic sprouting and capillary lumen formation modeled by human umbilical vein endothelial cells (HUVEC) in fibrin gels: the role of fibroblasts and Angiopoietin-1. Microvasc. Res. 66, 102–112.

Pardali, E., Ten Dijke, P., 2012. TGFβ signaling and cardiovascular diseases. Int. J. Biol. Sci. 8, 195–213.

Park, S.-Y., Kim, K.-H., Shin, S.-Y., Koo, K.-T., Lee, Y.-M., Seol, Y.-J., 2013. Dual delivery of rhPDGF-BB and bone marrow mesenchymal stromal cells expressing the BMP2 gene enhance bone formation in a critical-sized defect model. Tissue Eng. Part A 19, 2495–2505.

Park, Y.K., Tu, T.-Y., Lim, S.H., Clement, I.J.M., Yang, S.Y., Kamm, R.D., 2014. In vitro microvessel growth and remodeling within a three-dimensional microfluidic environment. Cell. Mol. Bioeng. 7, 15–25.

Qutub, A.A., Popel, A.S., 2009. Elongation, proliferation and migration differentiate endothelial cell phenotypes and determine capillary sprouting. BMC Syst. Biol. 3, 13.

Ribeiro, F.O., Gómez-Benito, M.J., Folgado, J., Fernandes, P.R., García-Aznar, J.M., 2015. In silico mechano-chemical model of bone healing for the regeneration of critical defects: the effect of BMP-2. Plos One 10, e0127722.

Rong, R., Wang, Y.-C., Hu, L.-Q., He, Q.-Q., Zhou, X.-F., Wang, T.-H., Bu, P.-L., 2015. Role of endogenous PDGF-BB in cultured cardiomyocytes exposed to hypoxia. Neuropeptides 50, 43–49.

Schreier, T., Degen, E., Baschong, W., 1993. Fibroblast migration and proliferation during in vitro wound healing. Res. Exp. Med. 193, 195–205.

Shamloo, A., Ma, N., Poo, M.-M., Sohn, L.L., Heilshorn, S.C., 2008. Endothelial cell polarization and chemotaxis in a microfluidic device. Lab Chip 8, 1292–1299.

Song, J.W., Munn, L.L., 2011. Fluid forces control endothelial sprouting. Proc. Natl. Acad. Sci. USA 108, 15342–15347.

Suwanadabol, P.A., Seedial, S.M., Shi, X., Zhang, F., Yamanouchi, D., Roenneburg, D., Liu, B., et al., 2012. TGF-B increases vascular smooth muscle cell proliferation through the Smad3 and ERK MAPK pathways. J. Vasc. Surg. 56, 446–454.

Theberge, A.B., Yu, J., Young, E.W.K., Ricke, W.A., Bushman, W., Beebe, D.J., 2015. Microfluidic multiculture assay to analyze biomolecular signaling in angiogenesis. Anal. Chem. 87, 3239–3246.

Tonnesen, M.G., Feng, X., Clark, R.A.F., 2000. Angiogenesis in wound healing. J. Investig. Dermatol. Symp. Proc. 5, 40–46.

Ucuzian, A.A., Gassman, A.A., East, A.T., Greisler, P., 2010. Molecular mediators of angiogenesis. Burn Care Res. 31, 1–28.

Vempati, P., Popel, A.S., Mac Gabhann, F., 2014. Extracellular regulation of VEGF: isoforms, proteolysis, and vascular patterning. Cytokine Growth Factor Rev. 25, 1–19.

Vickerman, V., Blundo, J., Chung, S., Kamm, R.D., 2008. Desing, fabrication and implementation of a novel multiparameter control microfluidic platform for three-dimensional cell culture and real-time imaging. Lab Chip 8, 1468–1477.

Vickerman, V., Kamm, R.D., 2012. Mechanism of a flow-gated angiogenesis switch: early signaling events at cell-matrix and cell–cell junctions. Integr. Biol. (Camb.) 4, 863–874.

Willette, R.N., Gu, J.L., Lysko, P.G., Anderson, K.M., Minehart, H., Yue, T., 1999. BMP-2 gene expression and effects on human vascular smooth muscle cells. J. Vasc. Res. 36, 120–125.

Zervantonakis, I.K., Hughes-Alford, S.K., Charest, J.L., Condeelis, J.S., Gertler, F.B., Kamm, R.D., 2012. Three-dimensional microfluidic model for tumor cell intravasation and endothelial barrier function. Proc. Natl. Acad. Sci. USA 109, 13515–13520.

Zuidema, J.M., Rivet, C.J., Gilbert, R.J., Morrison, F.A., 2014. A protocol for rheological characterization of hydrogels for tissue engineering strategies. J. Biomed. Mater. Res.—Part B Appl. Biomater. 102, 1063–1073.